Quantifying 3D building form effects on urban land surface temperature and modeling seasonal correlation patterns

Huifang Li [a,*], Yanan Li [a], Tao Wang [a], Zhihua Wang [b], Meiling Gao [c], Huanfeng Shen [a]

[a] *School of Resource and Environmental Sciences, Wuhan University, PR China*
[b] *School of Sustainable Engineering and the Built Environment, Arizona State University, USA*
[c] *School of Geology Engineering and Geomatics, Chang'an University, PR China*

ARTICLE INFO

ABSTRACT

Multiple factors regulate urban land surface temperature (LST), including land cover, climate, and urban form, among which urban form is now receiving more and more attention. Some studies have discussed the planar effects of urban form on LST, whereas less concern has been devoted to the vertical structure of urban areas, which can have a significant effect on heat redistribution. In this paper, we quantify the three-dimensional building form (3DBF) effects on LST captured by Landsat thermal sensors over four seasons by using a random forest (RF) regression method. The five 3DBF factors of building density (BD), building height (BH), sky view factor (SVF), frontal area index (FAI), and building shadow (BS) are calculated within a grid. The seasonal correlation of the 3DBF factors with LST is analyzed, and seven correlation patterns are modeled for the city of Wuhan in China. The results show that: 1) The best grid scale for the building form analysis in a city such as Wuhan is 180 m. 2) The 3DBF factors have a significant effect on urban LST over the four seasons. BD, BH and BS are the season-stable factors, among which BD has a heating effect, which reaches a maximum of 3.6 °C in spring, while BS has a cooling effect, which reaches −3.4 °C in winter. There is also a transition point for BH between heating and cooling at a height of 10 m. 3) SVF and FAI are season-varying factors, in which SVF has cooling effect, except in summer, while FAI also has a cooling effect, but not in winter. These findings will help us to understand how building form affects urban surface temperature, and will provide a reference for urban policy makers and planners in the future.

1. Introduction

It is projected by the United Nations [1] that nearly 70% of the world's population will live in cities by 2050, which is an increase from 54% in 2016. The importance of the urban thermal environment to human wellbeing continues to increase and has become the focus of public attention because of global warming and urban heat island effects. the urban thermal environment can be measured by air temperature (AT) and land surface temperature (LST), among which LST is directly related to the surface characteristics and reflects the high spatial and temporal variability of the surface thermal situation [2–4,5]. Nowadays, LST data can be conveniently obtained through satellite remote sensing, which benefits spatially continuous monitoring and the analysis of the urban thermal environment [6,7]. Many studies have now addressed urban LST and the related factors by the use of satellite data [8–10].

LST in urban areas is affected by multiple factors, including land cover, meteorological conditions, and urban form [9,11,12]. Among these factors, the effect of land cover, including green vegetation, water, and man-made impervious surfaces, has been extensively studied at different scales [13–16]. The effects of meteorological conditions are usually studied at large scales, such as global or regional scales, and the results can vary among cities with different climates [10,17]. Urban form refers to the composition and configuration of the different landscapes in a city, reflecting the spatial morphology of a city. Many landscape metrics, such as the percentage of landscape (PLAND), Shannon's evenness index (SHEI), and edge density (ED), are commonly used to quantify the effects of planar urban forms on LST. A strong correlation between LST and landscape metrics was reported in a case study in Shanghai, China [18], and significant relationships between the form of impervious surfaces and LST were found in the megacities of Southeast Asia [19]. It is now recognized that full knowledge of the

effects of urban form on LST is important for "thermal-environment-friendly" urban planning, especially for newly developed urban districts [20]. More investigation is therefore needed to establish the effects of urban form on LST, in both planar and vertical geometries.

The previous studies have mostly investigated the urban form in two dimensions by projecting buildings onto the horizontal plane [21]. However, urban form is practically made up of multiple buildings with varying densities and heights. Urban or street canyons are everywhere in urban areas, where a street is flanked by buildings on both sides, creating a canyon-like environment [22]. These building structures can change heat storage, reduce sky view, or modify airflow, which all affect urban temperature. Thus, vertical structures cannot be disregarded when depicting urban form and investigating its effects on LST. In this paper, the three-dimensional building form (3DBF) factors are used to describe the realistic urban form in the central area of a major city, and the effects of the 3DBF factors on LST are investigated at fine spatial resolutions from 30 m to 210 m.

3DBF refers to the spatial structure and composition of buildings [23, 24], and it mainly affects LST by altering the incident solar energy and air ventilation [25]. Typical 3DBF factors include building density (BD), building height (BH), sky view factor (SVF), frontal area index (FAI), and building shadow (BS, referring to the shadow area ratio) [26–28]. The effects of some of these 3DBF factors on LST have been investigated using both linear and nonlinear models, among which the nonlinear models have been shown to perform better than the linear models, such as random forest, gradient boost regression trees and convolutional neural network [29,30]. However, urban surface temperature is actually impacted by multiple 3DBF factors simultaneously, and the impacts may be dependent on seasons, day/night, regions and scales. Therefore, new methods rather than simple linear models are required to analyze the comprehensive quantitative effects of multiple 3DBF factors on LST, for which random forest (RF) is a good choice [31,32]. RF is a strong multivariate analysis tool, does not assume linearity and has been demonstrated to be the best among six regression models in a previous study [30].

In this paper, with the central area of the city of Wuhan in China selected as the study area, satellite data and building morphological data were utilized to obtain LST and 3DBF information over the four seasons of the year. Five 3DBF factors were calculated and according to that the building form was classified into six categories. RF regression model was used to explore the comprehensive quantitative effects and the importance of the multiple factors. As we focus on 3DBF in this paper, the coefficient of determination (R^2) only reflects the influence of the building form among multiple LST-related factors. Furthermore, the seasonal correlation patterns between 3DBF and LST were extracted and modeled. The results will provide a theoretical reference for the rational urban planning of 3DBF factors and the improvement of the urban thermal environment.

2. Related works

2.1. Urban form measure

The urban form or urban morphology has been focused on by many studies and its effects on the urban environment have also been validated [33]. The urban form is usually measured from two aspects: 2-dimensional (2D) urban form and 3-dimensional (3D) urban form. The 2D urban form describes the spatial patterns of the major zones of a city, such as buildings, trees, and roads [20]. Corresponding to each class of zone, the landscape metrics, including percentage of landscape area (PLAND), edge density (ED), patch density (PD), landscape shape index (LSI) and et al., are used to measure the 2D building form. The 3D urban form is the extension of 2D to the vertical direction, mainly describing structures of buildings or trees. The measures consist of density, height, volume, sky view factor (SVF), shadow footprint (SF) and some specific factors for buildings such as floor area ratio (FAR) and frontal area index

(FAI) [34,35]. We focus on the 3D spatial morphology of buildings in this paper. Considering the building geometry and its interaction with the environment, five widely used factors are therefore selected, including building density (BD), building height (BH), SVF, FAI and building shadow area ratio (BS).

2.2. Effects of urban form on thermal environment

Though it is evident that urban form has impacts on urban thermal environment, the impacting mechanism of each factor is different and their impacts on air temperature and land surface temperature are different or even opposite. 3D building morphology indicators were reported stronger associations with urban air temperature than 2D indicators, which diverges from those conclusions according to the surface temperature studies [36]. 2D building structures showed more effects on urban thermal environment than 3D structure during the day, but an opposite trend occurred at night [20,37]. For a specific urban form indicator, different results were also discovered. Taking the most typical 3D indicator BH for example, it is positively related to air temperature [38], while negatively to surface temperature [20,37]. This phenomenon can be attributed to the difference of heating and cooling mechanisms between air and surface temperatures.

We focus on the urban thermal environment delineated by land surface temperature in this paper, which is directly related to the received solar radiation and physical properties of the surfaces and meanwhile affected by the urban form. Besides BH, BD and SVF are the two mostly discussed indicators. BD is positively related to LST which is commonly approved [29,36,38]. The effect of SVF is complicated and context-dependent, for which both negative and positive relations were reported [20]. It is very necessary to analyze the effect of SVF for a case study. Moreover, shadows have been mentioned many times to explain the cooling effects of high-rise buildings, and a specific research on the relation of building shadows and LST also verified the cooling effect reaching 3.16 K in summer [39]. But the multi-variable analysis including building shadows related to LST has not been conducted. Another 3D factor having influence on heat convection is FAI, as it is an important indicator of the barriers of the urban ventilation [34]. It was reported that 10% increase in FAI can result in a 2.5% decrease in the wind speed ratio in Hong Kong's high-density areas, further changing the air temperature and UHI [40]. However, the effects on LST have not been clear.

Therefore, the 3D urban form and its relation to LST have received lots of attentions recently, but the sophisticated affecting mechanisms of each factor and their mutual influence, marginal effect and quantitative impact deserve further and deeper studies.

3. Study area and data

3.1. Study area

Wuhan is the capital of Hubei province in China, and is located between 29°58′–31°22′ N and 113°41′–115°05′ E. The location of the study area is shown in Fig. 1. As the fifth-largest city in China, with an area of about 8500 km^2 and over 10 million population, Wuhan is known as one of China's four "oven cities", where summertime temperatures can soar to 40 °C. In Wuhan, summer is the longest season, with almost 135 days a year.

We selected the central area of the city of Wuhan as the study area, located within the second ring road, as shown in Fig. 1(c), where there are both dense buildings and multiple types of buildings, and the building form is likely an important factor affecting the urban LST.

3.2. Data

Building data, meteorological parameters, and remote sensing images of Wuhan in 2018 were used in this study. The building
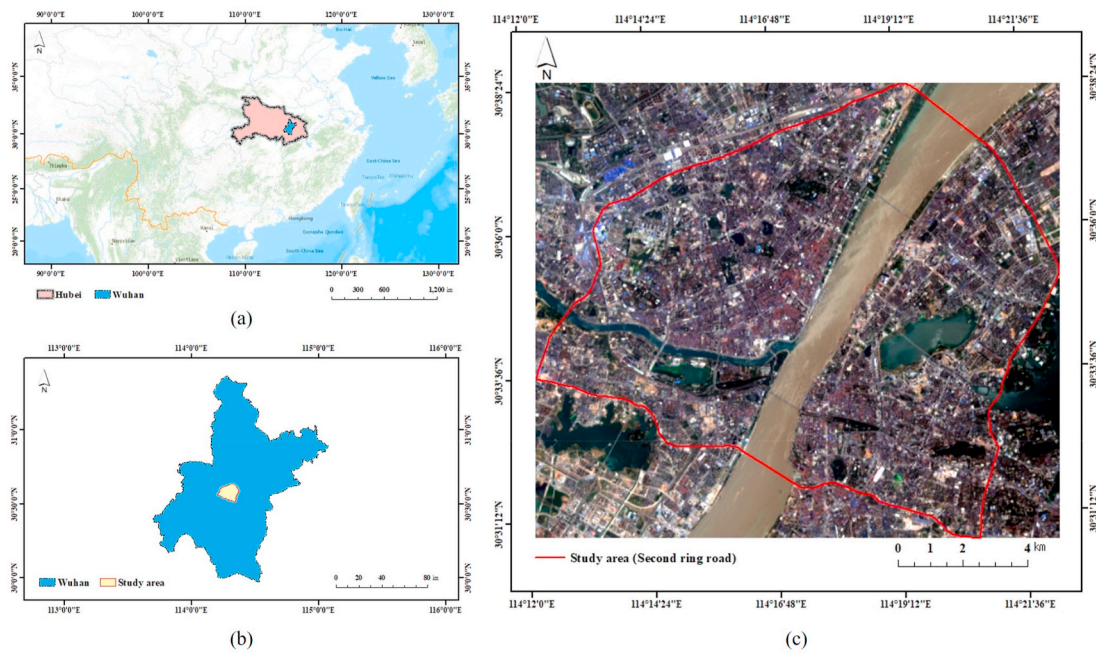
Fig. 1. Location of the study area. (a) Geographical location of the city of Wuhan in China. (b) Geographical location of the study area in Wuhan. (c) Landsat 8 true-color image of the study area on July 29, 2018.

morphological data were in vector format, and included the location, shape, and height of all the buildings in central Wuhan, and were derived from a public data sharing platform (https://www.metrodata.cn). A part clipped from the building data is shown in Fig. 2, in which four levels of building height are rendered in different colors. The meteorological parameter used in this study was the wind direction, which was used to establish the predominant wind direction of the city and to support the calculation of the 3DBF factor (FAI).

Band 10 of the Landsat 8 (10.60–11.19 μm) and band 6 of Landsat 7 (10.40–12.50 μm) were chosen for retrieving the LST. The spatial resolutions of the Landsat 8 and Landsat 7 thermal infrared bands are 100 m and 60 m respectively, and they have been officially resampled to 30 m using the cubic convolution algorithm by the U.S. Geological Survey [41]. Cloud-free Landsat thermal images of four seasons in 2018 captured on April 08, July 29, September 15, and January 10 were collected, in which the winter data were from Landsat 7 and the other

data were from Landsat 8 because of the cloud cover problem. Due to the failure of the scan line corrector (SLC) on Landsat 7 in 2003, a method was needed to recover the missing information in the winter data, for which the multi-temporal regression and regularization method was used in this study [42]. LST data information and weather information captured by the meteorological station locating in the central city on that date are listed in Table 1.

4. Methods

4.1. Calculation of 3D building form factors

The five typical 3D building form (3DBF) factors of building density, building height, sky view factor, frontal area index, and building shadow, were chosen to represent the building form. These factors were defined as follows and calculated by rectangular grids [43].

Fig. 2. Building data of Wuhan rendered by building height.

Table 1
The weather information of the day.

Season	Sensor	Date	Path/row	Cloud cover (%)	Air temperature (°C)	Relative humidity (%)	Wind speed (m/s)	Global solar radiation (MJ/m²)
Spring	Landsat8	2018/04/08	123/39	8.94	17.0	46.3	1.6	11.02
Summer	Landsat8	2018/07/29	123/39	21.58	30.9	71.5	1.0	13.43
Autumn	Landsat8	2018/09/15	123/39	3.11	27.5	66.3	2.3	11.06
Winter	Landsat7	2018/01/10	123/39	1.00	5.2	58.2	0.8	4.37

Building density (BD): the ratio of the total area of a building to the area of the grid. A high building density means high intensity of land use and development.

Building height (BH): the weighted average height of the buildings within the grid. The base area of each building is used to weight the height.

Sky view factor (SVF): the fraction of the overlying hemisphere occupied by the sky, which ranges from 0 (no sky visible) to 1 (no horizon obstructions visible). This factor measures the extent of the 3D open space, and can be expressed as:

$$SVF = 1 - \sum_{i=1}^{N} \sin^2 \beta i \left(\frac{\alpha i}{360°} \right) \qquad (1)$$

where N is the total number of sectors obscured by obstacles in the sky hemisphere, and α_i and β_i are the azimuth angle and maximum building height angle for each sector, respectively [44].

Frontal area index (FAI): the integration of $FAI(\theta)$ weighted by the wind direction frequency $P(\theta)$, which can be expressed as:

$$FAI = \sum_{n=1}^{16} P(\theta) FAI(\theta) \qquad (2)$$

where $FAI(\theta)$ is the ratio of a projected windward building area A_{proj} to a unit horizontal area A_T, expressed as $FAI(\theta) = A_{proj}/A_T$, which can be used to describe the surface roughness of the study area by grid [45]. θ is the wind direction, which is usually measured in 16 directions. A large *FAI* means that the buildings represent great obstacles for the wind, which may reduce the air and heat convection between the city proper and the suburb.

Building shadow (BS): the ratio of the building shadow area to the unit horizontal area. Clearly, BS is a time-varying factor, for which the time is consistent with the imaging time of the remote sensing thermal data.

4.2. Building form categories

We defined six building form categories to clearly map the spatial distribution of the buildings in the city by considering three main factors, SVF, BD and BH. The classification rules were consistent with those of the local climate zones defined by Oke in 2012 [46], which were widely approved and adopted to analyze the urban form. The categories and classification rules are listed in Table 2. According to the current status of the buildings in the city, SVF and BD were divided into two levels respectively, i.e., open form with BD ≤ 40% and SVF ≥ 0.6, and

compact form with BD > 40% or SVF < 0.6. BH was divided into three levels, i.e. low-rise form with 3 m ≤ BH ≤ 10 m, mid-rise form with 10 m < BH ≤ 25 m, and high-rise form with BH>25 m. Six building form categories could then be obtained by comprehensively combing the SVF, BD and BH, i.e., OH (open high-rise), OM (open mid-rise), OL (open low-rise), CH (compact high-rise), CM (compact mid-rise) and CL (compact low-rise). The different building categories can represent the different geometrical morphologies and energy balances of the urban surface, which can support the local-scale climate investigation of a region.

4.3. Land surface temperature retrieval

In this study, the emissivity-based method was employed to retrieve the LST [8], in which no real-time atmospheric profile data are required and only the top-of-atmosphere (TOA) radiance and normalized difference vegetation index (NDVI) are necessary. Based on Planck's radiation formula, the relationship between the LST and the brightness temperature can be expressed as [47]:

$$TS = \frac{T_B}{1 + (\lambda T_B / \alpha) \ln \varepsilon} \qquad (3)$$

where T_S refers to the LST; T_B is the effective at-sensor brightness temperature in Kelvin; λ is the wavelength of the emitted radiance in meters (for Landsat 7, $\lambda = 11.269$μm and for Landsat 8, $\lambda = 10.904$μm); and is the surface emissivity, which can be calculated based on the vegetation index by a mature model [48].

The brightness temperature T_B can be converted from the TOA radiance L_λ of the Landsat thermal infrared band [49]:

$$TB = \frac{K_2}{\ln(\frac{K_1}{L_\lambda} + 1)} \qquad (4)$$

where K_1 and K_2 are calibration constants. For the Landsat 8, K_1 is 774.89 W/(m² sr μm) and K_2 is 1321.08 K; for the Landsat 7, K_1 is 666.09 W/(m² sr μm) and K_2 is 1282.71 K.

4.4. Random forest regression

Random forest (RF) is a kind of nonlinear, nonparametric machine learning method, which was originally proposed for prediction and regression in various fields [50,7]. The learning process is based on decision trees, in which the variable selection is totally random, so that it is insensitive to multivariate collinearity. RF can also provide an importance score to each factor, which can be used to quantify the contribution of each variable [51]. In a study of the effect of urban characteristics on LST, RF showed the highest accuracy among six linear and nonlinear models [30].

In this study, the 3DBF factors were taken as the independent variables, and LST was taken as the dependent variable to model the random forest. In the modeling process, 75% of the data were randomly selected as the training dataset, and 25% were used as the test dataset. The optimal numbers of trees for spring, summer, autumn, and winter were determined as being 200, 245, 245, and 170, respectively, which was established by testing from 100 to 500 at intervals of 5. Based on the modeled random forest, the contribution of each 3DBF factor to LST could be quantified and ranked. To further explore the effects of each

Table 2
Definition of the building form categories in Wuhan.

Building category	SVF	BD (%)	BH (m)
OH (open high-rise)	≥0.6	<40	>25
OM (open mid-rise)	≥0.6	<40	[10, 25]
OL (open low-rise)	≥0.6	<40	[3, 10]
CH (compact high-rise)	<0.6	≥40	>25
CM (compact mid-rise)	<0.6	≥40	[10, 25]
CL (compact low-rise)	<0.6	≥40	[3, 10]

factor on LST, partial dependence plots (PDPs) were drawn for all the independent variables [52,53]. In PDPs, the regression function is fixed at a tested 3DBF factor and averaged over the others, reflecting the relationship between LST and the test factor, whether the relationship is linear or nonlinear. Moreover, the peak values in the PDPs represent the maximum heating or cooling degree of the test factor.

5. Results and analysis

5.1. Optimal grid scale

Since the 3DBF factors and LST were measured in square grids, the best grid scale for the RF regression model needed to be determined before the analysis. Considering the urban building size and the dataset volume, seven grid scales ranging from 30 m to 210 m with a step of 30 m were used to calculate the corresponding 3DBF factors and LST, and to establish the RF regression model. The overall determination coefficient (R^2) and root-mean-square error (RMSE) of the test dataset were adopted as the evaluation indices for the model performance. The experimental results for the four seasons are shown in Table 3.

According to the R^2 and RMSE values, the model accuracy rises gradually along with the increase of the grid scale in the four seasons. Specifically, the grid scale is different when the highest R^2 and lowest RMSE values are reached in the different seasons. For spring and summer, R^2 reaches its highest value when the grid size is 210 m, and RMSE reaches its lowest value when the grid size is 180 m. Meanwhile for autumn and winter, R^2 reaches its highest value when the grid size is equal to 180 m, and RMSE reaches its lowest values when the grid size is 210 m. By comprehensively considering the performance with regard to R^2 and RMSE in the different seasons and the size of the studied central urban area, 180 m was taken as the optimal grid scale for the urban form analysis, which is where the inflection point appears for both metrics.

From Table 3, it can be seen that the highest R^2 is above 0.4 in all four seasons at the optimal grid scale, which is low as only the 3DBF factors participate in the regression modeling. The building form accounting for more than 40% of the contribution to LST can be considered as very considerable when no other factors are involved. This suggests that building form plays an important role in affecting LST in a city.

5.2. Building form spatial distribution

Fig. 3 presents the maps of the 3DBF factors and the building form category obtained according to the rules defined in Table 2. In the maps of BD, SVF, and FAI in summer and BS in summer, the five levels are sliced by the standard deviation, and the four levels in the map of BH in summer are sliced according to the criteria defined by Oke [46]. The more saturated red represents a higher value. The distributions of these five factors show obvious spatial differences. BD shows aggregation in the urban center, and also along the Yangtze River, while BH shows some dispersed hot spots deviating from the urban center. This is consistent with the urban development of Wuhan, in which the old town with lots of CL and CM buildings located in the city center, and the newly

developed districts with OH buildings far away from the center, corresponding to the building form category shown in Fig. 3(f). In Fig. 3(c), lots of high SVF pixels locate by the riverside and the lakeside, because of the high openness of the large water surface. FAI and BS are evenly dispersed in the study area, with no significant aggregation.

5.3. Seasonal correlation analysis

5.3.1. Relative importance ranking

The relative importance of the five 3DBF factors to LST in the four seasons at a grid scale of 180 m is sho0wn in Fig. 4. The factors whose importance ranks in the top two are marked in red, and the others are marked in blue. The ranking in spring is similar to that in summer, and the ranking in autumn is similar to that in winter. BD and BH are the two most important variables in spring and summer, and BD and BS are the two most important variables in autumn and winter. BD ranks first in spring, summer, and autumn, suggesting that BD is the most important factor among the five 3DBF factors. BH is important in spring and summer, but is surpassed by BS in autumn and winter, which means that shadows can effectively reduce LST when the sun elevation is low and the shadow area is large. Compared with the above three factors, the effects of SVF and FAI on LST are small in all four seasons.

5.3.2. Correlation patterns

The partial dependence plots (PDPs) of the five 3DBF factors in the four seasons are shown in Fig. 5. The PDP reflects the LST change along with the 3DBF factor, in which the solid blue curve represents the mean marginal effect, the dashed red line represents a zero effect, and the shaded region indicates the confidence level. It can be seen that some factors show similar trends in the different seasons, but some others do not. According to this, the five 3DBF factors were divided into two categories: season-stable factors (BD, BH, and BS) and season-varying factors (SVF and FAI). We summarized the different correlation patterns for the different factors based on Fig. 5, and extracted their maximum effects on LST in the four seasons, as listed in Table 4 and Table 5.

For the season-stable factors, the three patterns, as listed in Table 4 (*ascent*, *fluctuated descent*, and *descent*) are summarized for BD, BH, and BS. Among the different factors, BD shows a significant positive correlation with LST in all four seasons. The maximum LST changes attributed to BD in the four seasons are 3.60 °C, 2.60 °C, 2.4 °C, and 1.60 °C, which are the largest among the five 3DBF factors in spring, summer, and autumn, and the second largest in winter. This verifies the importance of BD quantitatively. BH shows the fluctuated descent pattern, in which an obvious turning point appears when BH is approximately equal to 10 m. Similar finding was reported by a study in the Beijing Olympic Park, China that the positive influence of BH reached a maximum at a height of 15 m [29]. Also, this nonlinear relationship between BH and LST shows the same trend with a prior modeling and theoretical work by Song and Wang, which illustrates the radiative trapping effect and shading effects in street canyons elaborately (Song and Wang, 2015). Based on that, it can be deduced that the governing mechanism for LST

Table 3
R^2 and RMSE of the RF model at different grid scales in the four seasons.

Grid Scale (m)	R^2				RMSE			
	Spring	Summer	Autumn	Winter	Spring	Summer	Autumn	Winter
30	0.27	0.22	0.24	0.30	2.26	1.05	1.20	1.22
60	0.35	0.29	0.32	0.39	1.96	0.93	1.00	1.02
90	0.38	0.34	0.36	0.42	1.82	0.86	0.89	0.90
120	0.41	0.38	0.37	0.42	1.74	0.83	0.84	0.83
150	0.45	0.42	0.39	0.43	1.61	0.79	0.78	0.76
180	0.47	0.46	**_0.42_**	**_0.43_**	**_1.53_**	**_0.74_**	0.72	0.69
210	**_0.49_**	**_0.49_**	0.41	0.41		0.74	**_0.70_**	**_0.67_**
				1.54				

Note: bold/underline indicates the best results.
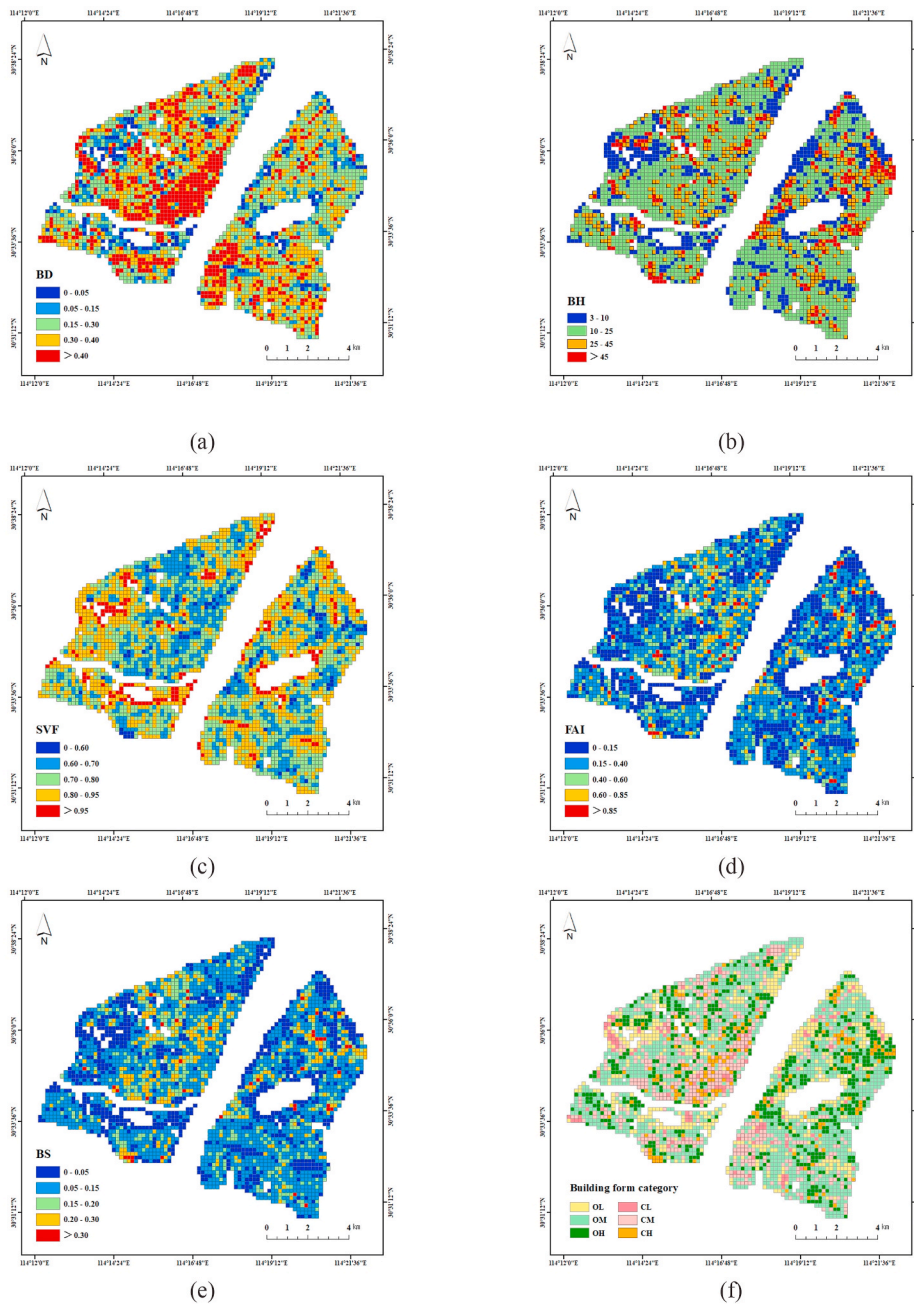
Fig. 3. Building form of central Wuhan at a grid scale of 180 m. (a) BD, (b) BH, (c) SVF, and (d) FAI in summer. (e) BS in summer. (f) Building form category. Note: the data ranges of BD, SVF, FAI, and BS are all normalized to [0,1].

change is different at different heights in a city. When building height is lower than a turning point, building surface tends to be warmer since more heat is trapped. In contrast, buildings with higher height are cooler because of larger shaded areas, which show significant negative correlations with LST in all four seasons as list in Table 3. The maximum impact of BS on LST is −1.20 °C, −0.40 °C, −1.60 °C, and −3.40 °C in spring, summer, autumn, and winter, respectively. It can therefore be seen that the strongest cooling effect of BS is in winter and the weakest is in summer, which can be also attributed to the shaded areas.

For the season-varying factors, two different patterns—*gradual descent* and *inverted U*—are apparent for SVF, while two other patterns—*tailed U* and *gradual ascent*—are apparent for FAI, as shown in Table 5. It can be seen that SVF has a negative impact on LST in spring, autumn, and winter, because a larger SVF indicates more efficient air flow and heat conduction. The maximum cooling effects are −0.5 °C,

−0.35 °C, and −0.38 °C, respectively, which are not significant effects when compared to the other factors. Differently, SVF shows a complex correlation with LST in summer, like an inverted U shape, in which it is positive first and then changes to negative. The maximum effect is 0.4 °C. We speculate that the initial positive correlation in summer can be attributed to more incident sunlit energy caused by larger SVF, helping rise LST, and the subsequent negative correlation may be due to more open space facilitating the air flow in street canyons via convection, helping reduce LST. Our results are consistent with a case study of Beijing, which found that building-based SVF raises the LST in summer when it is less than 0.8, but reduces the LST when it is larger [29]. So far, it has been commonly recognized that the effect of SVF on LST is complicated and context-dependent [20].

FAI itself is a season-varying variable, and it shows two different correlation patterns with LST over the four seasons, i.e., tailed U and
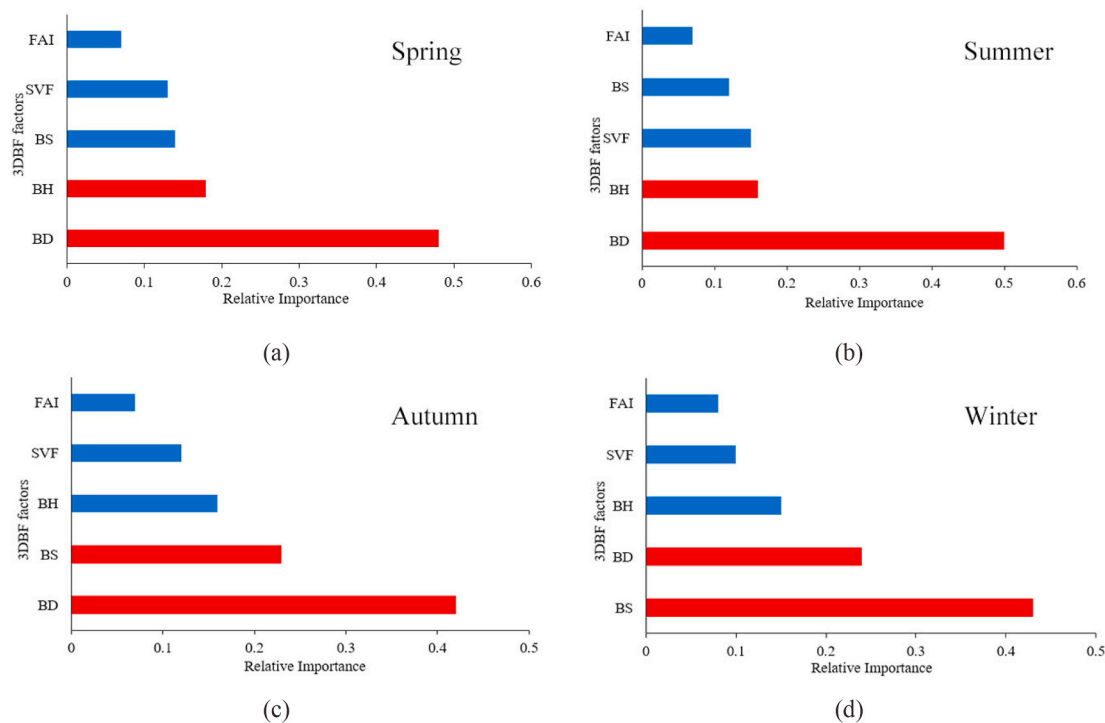
Fig. 4. Sorting chart of the relative importance of the five 3DBF factors in each season. The factors whose relative importance ranks in the top two are marked in red, and the others are marked in blue. (a) Spring. (b) Summer. (c) Autumn. (d) Winter.

gradual ascent. The former represents a cooling effect in spring, summer, and autumn, while the latter represents a heating effect in winter, although the maximum effect is no larger than 0.3 °C in any season. To date, few studies have explained the seasonal variation of the FAI effect reasonably. In this paper, we have tried to explain this from the specific building forms related to FAI.

The variation of FAI should be related to BD and BH, where BD has a heating effect while BH has a cooling effect in the urban area. We calculated the Pearson correlation coefficients between BD and FAI, i.e., $C_{FAI,\ BD}$, as well as BH and FAI, i.e., $C_{FAI,\ BH}$, in the four seasons, as shown in Table 6, where RD represents the relative difference calculated by $(C_{FAI,\ BH} - C_{FAI,\ BD})/C_{FAI,\ BD}$. It can be seen that FAI has about a 10% higher correlation with BH than BD in the four seasons, and the largest RD appears in summer, when the largest maximum effect of FAI, i.e., −0.30 °C, as shown in Table 5, appears correspondingly. This suggests that the cooling effect caused by BH dominates the impact of FAI in summer, and also spring and autumn. In contrast, the smallest RD, i.e., 10.07%, appears in winter, when FAI shows a heating effect, suggesting that the effect of BD dominates the impact of FAI in winter. Therefore, we speculate that the effect of FAI can be considered as a trade-off between BD and BH in the different seasons. Furthermore, local climate, heat conduction, or heat storage could also be reasons for the effect of FAI on LST, which is worth further investigation, and will need higher-resolution data support.

6. Discussion

6.1. The impacts of building form on LST and the optimal scale

Based on the urban energy balance theory, the energy absorbed by the surface is balanced by heating up the air above the surface, evaporation and heat storage in surface materials when the heat advection is not considered [20,54]. The urban form can affect the urban thermal environment through modifying the partitioning energy in the energy balance process. This study reveals that 3D building forms can explain more than 40% LST variation by using the random forest model at some

scale. BD has the strongest annual mean impact on LST, while FAI has the smallest impact on LST. BD describes the percentage of the building footprint in a grid, which is also in accordance with the covering ratio of the impervious surfaces, reflecting the physical property of the surfaces. The building class has the largest impact on urban LST variation at a fine scale in the comparison analysis of different urban functional zones [20]. FAI is an important index that reflects the wind permeability of urban buildings, an important indicator for the urban ventilation [34]. In some previous research, air temperature was strongly affected by the near-ground air flow, whereas the surface temperature was more affected by the short-wave radiation and surface materials. That can be the reason for the weak influence of FAI in our study. The effects of BH, BS and SVF are less than BD in most cases, but their ranks switch among different seasons. That is because BS is a time-dependent variable, increasing along with the decreasing of the solar elevation, while BH and SVF are stable variables.

The effects of building form on LST were discussed at grid scale in this study. The LST of those pixels in a grid were aggregated and averaged, and also building form factors were calculated in that grid. Seven grid scales ranging from 30 m to 210 m were discussed in the experiments. The overall tendency is that the larger the grid is, the higher the modeling accuracy is before the grid scale is not larger than 180 m. With the increase of the grid scale, the modeling accuracy may continue to increase in some seasons but the number of the available grids will not be enough for the modeling. By comprehensively considering the accuracy, the seasons and the grid numbers, 180 m was determined as the optimal grid scale in this study.

6.2. The marginal effects of 3DBF factors and the seasonal variation

Higher BD means more heat storage and fewer evaporation [34], causing higher LST. The heating effect of BD is very stable in our study, which is in line with a lot of previous studies [29,34,36]. BH is negatively related to LST overall, although short accent tendency appears when the building height is lower than 10 m, which is opposite to the study on the air temperature. It can be attributed to two reasons. One is
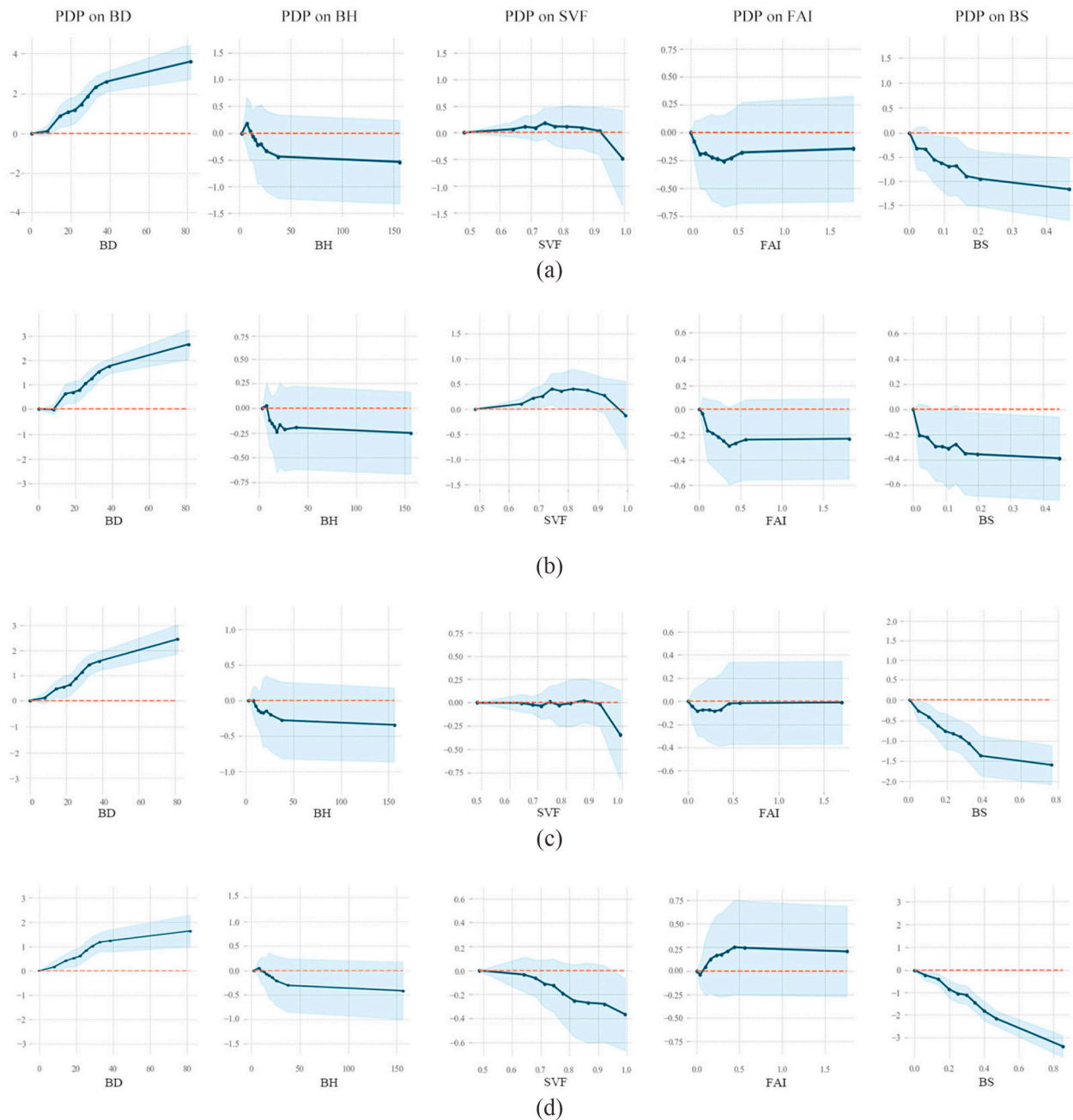
Fig. 5. PDPs of the five 3DBF factors in the four seasons. (a) Spring. (b) Summer. (c) Autumn. (d) Winter.

that high-rise buildings shield more solar radiation and cast more shadows, cooling the surface. Another is that high-rise buildings improve the surface roughness which may generate mechanical turbulence and thereby enhances the convective heat dissipation [20].

The cooling effect of shadows is commonly considered as the main reason [35,38]. Hence the BS factor indicating the building shadow percentage in a grid was taken as an important building form measure in this study. Results show that BS plays important role in decreasing LST especially in autumn and winter, when the shadow areas are larger because of the lower solar elevation. This is in line with a previous study of the seasonal effect of building shadows on urban LST in Beijing, which suggested that LST distribution in winter was strongly affected by BS [39]. The discrepancy is that the quantitative analysis in that study shows that the lowest cooling occurred on pure impervious pixels totally covered by BSs in winter. That may be attributed to the different climate of study areas, as well as the joint effect of BH and BS, in which the effect

of BH is often explained by the effect of shadows casted by buildings. We explored multiple building form factors in this paper, whereas only BS was discussed for pure pixels in Yu et al. [39].

The impact of SVF on LST is complicated, for which some contradictor results have been reported [55–57]. Our study reveals that the main marginal effect of SVF is negative, especially when SVF is larger. SVF affects the LST through two ways: ventilation and incoming solar radiation. Larger SVF means better air circulation in densely built environment thereby lower temperature, meanwhile more incoming solar radiation into the surface resulting to higher temperature. The final impact of SVF is determined by the trade-off between these two processes. Therefore, the heating effect on LST occurs in summer, when the solar radiation is the greatest in a year. By affecting the urban ventilation, higher FAI means less air circulation thereby higher temperatures [35]. One the other hand, FAI is positively related to BH [29], and BH has negative effects on LST, which is an important discrepancy between

Table 4

Correlation patterns of the season-stable factors and their maximum effect (°C) on LST.
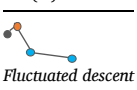
Pattern	BD (+)	BH (−)	BS (−)
	Ascent	*Fluctuated descent*	*Descent*
Spring	3.60	−0.50	−1.20
Summer	2.60	−0.25	−0.40
Autumn	2.40	−0.30	−1.60
Winter	1.60	−0.40	−3.40

Note: The plus sign +means positive correlation, while the minus sign − means negative correlation. In the patterns, a gray point represents zero effect, an orange point represents a heating effect, and a blue point represents a cooling effect.

Table 5

Correlation patterns of the season-varying factors and their maximum effect (°C) on LST.
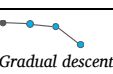
Pattern	SVF		FAI	
	Gradual descent	*Inverted U*	*Tailed U*	*Gradual ascent*
Spring	−0.50		−0.25	
Summer	0.40		−0.30	
Autumn	−0.35		−0.10	
Winter	−0.38		0.25	

Note: The patterns correspond to the seasons with same background color in the table.

Table 6

Pearson correlation coefficients between FAI and BD, FAI and BH, and their relative differences in the four seasons.

	$C_{FAI, BD}$	$C_{FAI, BH}$	RD
Spring	0.4449	0.4913	10.43%
Summer	0.4433	0.4902	10.58%
Autumn	0.4414	0.4860	10.11%
Winter	0.4421	0.4866	10.07%

air temperature and LST. By comprehensively considering these two aspects, seasonal variation is also found for the effect of FAI. Except winter, the cooling effect occurs in the other seasons, while the ventilation may be a more important factor for the LST in winter.

6.3. Limitations

The quantitative effects of 3D building form factors on LST were explored, as well as their seasonal variation and correlation patterns in this paper. There are still some limitations deserving further studies. First, the LST data was derived from the satellite observation at the top of a city, which may ignore the vertical surfaces and introduce bias for knowing the real thermal environment especially in the densely built areas. Second, pixels of satellite data are usually mixing of multiple classes of land surfaces, from which the temperature of specific building roofs is hardly extracted. Third, the analysis was conducted in one city and the climate conditions were not considered. In future research, multi-source data should be fused to represent the surface temperature more comprehensively in a finer scale, such as UAV (unmanned aerial vehicle) captured surface temperature data. Even some microclimate simulation model may be integrated with observation data to understand the urban thermal environment deeper. On the other hand, similar research should be conducted in other cities with different climate and arid-humid conditions, as UHI effect varies across geographic regions.

7. Conclusions

In this paper, the effects of 3DBF factors on LST in central Wuhan have been quantified at a fine grid scale by the use of an RF regression model, and the different correlation patterns have been modeled. Four conclusions can be made from the results. Firstly, we found that the optimal grid scale for the analysis of 3DBF effects on LST using RF was 180 m in central Wuhan. Secondly, the 3DBF effects on LST are significant, and can account for more than 40% of the contribution to LST variation. Thirdly, BD, BH, and BS are season-stable factors, which show ascent, fluctuated descent, and descent correlation patterns with LST over the four seasons. BD has the strongest heating effect of 3.6 °C in spring, while BS has the strongest cooling effect of −3.4 °C in winter. Fourthly, SVF and FAI are season-varying factors, which have different correlation patterns with LST in the different seasons. SVF has a cooling effect in spring, autumn, and winter, and a heating effect in summer. FAI comes last in the relative importance ranking, and it has a cooling effect in spring, summer, and autumn, and a heating effect in winter. These findings confirm that the effects of 3DBF factors on LST vary elaborately in urban areas. Furthermore, these findings will provide a reference for a better understanding of the urban heat island effect and the establishment of mitigation policies.

Declaration of competing interest

The authors declare that they have no known competing financial interests or personal relationships that could have appeared to influence the work reported in this paper.

References

[1] United Nations (UN), World Urbanization Prospects: the 2018 Revision, The United Nations' Department of Economic and Social Affairs - Population Division, New York, 2019, p. 126.

[2] R.A. Memon, D.Y.C. Leung, C. Liu, A review on the generation, determination and mitigation of Urban Heat Island, J. Environ. Sci. 122 (2008), 130.

[3] H. Shen, L. Huang, L. Zhang, et al., Long-term and fine-scale satellite monitoring of the urban heat island effect by the fusion of multi-temporal and multi-sensor remote sensed data: a 26-year case study of the city of Wuhan in China, Remote Sens. Environ. 172 (2016) 109–125.

[4] Q. Weng, Thermal infrared remote sensing for urban climate and environmental studies: methods, applications, and trends, ISPRS J. Photogrammetry Remote Sens. 64 (2009) 335–344.

[5] B. Wilson, Urban form and residential electricity consumption: evidence from Illinois, USA, Landsc. Urban Plann. 115 (2013) 62–71.

[6] Y. Fei, E.B. Marvin, Comparison of impervious surface area and normalized difference vegetation index as indicators of surface urban heat island effects in Landsat imagery, Remote Sens. Environ. 106 (2007) 375–386.

[7] L. Breiman, Random forests, Mach. Learn. 45 (2001) 5–32.

[8] X.L. Chen, H.M. Zhao, P.X. Li, et al., Remote sensing image-based analysis of the relationship between urban heat island and land use/cover changes, Remote Sens. Environ. 104 (2006) 133–146.

[9] S. Du, Z. Xiong, Y.-C. Wang, et al., Quantifying the multilevel effects of landscape composition and configuration on land surface temperature, Remote Sens. Environ. 178 (2016) 84–92.

[10] M. Gabriele, F. Simone, S. Markus, et al., Magnitude of urban heat islands largely explained by climate and population, Nature 573 (2019).

[11] M. Gao, F. Chen, H. Shen, Efficacy of possible strategies to mitigate the urban heat island based on urbanized high-resolution land data assimilation system (u-HRLDAS), J. Meteorol. Soc. Japan. Ser. II. 97 (2019).

[12] Y. Zhang, A.T. Murray, B.L. TurnerII, Optimizing green space locations to reduce daytime and nighttime urban heat island effects in Phoenix, Arizona, Urban Plan 165 (2017) 162–171.

[13] A. Dimoudi, M. Nikolopoulou, Vegetation in the urban environment: microclimatic analysis and benefits, Energy Build. 35 (2003) 69–76.

[14] A. Elmes, J. Rogan, C. Williams, et al., Effects of urban tree canopy loss on land surface temperature magnitude and timing, ISPRS J. Photogrammetry Remote Sens. 128 (2017) 338–353.

[15] C.M. Hsieh, H.-C. Huang, Mitigating urban heat islands: a method to identify potential wind corridor for cooling and ventilation, Comput. Environ. Urban Syst. 57 (2016) 130–143.

[16] R.B. Xiao, Z.Y. Ouyang, H. Zheng, et al., Spatial pattern of impervious surfaces and their impacts on land surface temperature in Beijing, China, J. Environ. Sci. 19 (2007) 250–256.

[17] K.E. Trenberth, D.J. Shea, Relationships between precipitation and surface temperature, Geophys. Res. Lett. 32 (2005).

[18] J. Li, C. Song, L. Cao, et al., Impacts of landscape structure on surface urban heat islands: a case study of Shanghai, China, Remote Sens. Environ. 115 (2011) 3249–3263.

[19] R.C. Estoque, Y. Murayama, S.W. Myint, Effects of landscape composition and pattern on land surface temperature: an urban heat island study in the megacities of Southeast Asia, Sci. Total Environ. 577 (2017) 349–359.

[20] X. Huang, Y. Wang, Investigating the effects of 3D urban morphology on the surface urban heat island effect in urban functional zones by using high-resolution remote sensing data: a case study of Wuhan, Central China, ISPRS J. Photogrammetry Remote Sens. 152 (2019) 119–131.

[21] G. Han, Z. Cai, Impact of mountain urban Park form on cooling effect, J. Human Settle. West China 31 (2016) 61–68.

[22] M. Nunez, T.R. Oke, The energy balance of an urban canyon, J. Appl. Meteorol. 16 (1977) 11–19.

[23] C. Yin, M. Yuan, Y. Lu, et al., Effects of urban form on the urban heat island effect based on spatial regression model, Sci. Total Environ. 634 (2018) 696–704.

[24] A. Middel, K. Hab, A.J. Brazel, et al., Impact of urban form and design on mid-afternoon microclimate in Phoenix Local Climate Zones, Landsc. Urban Plann. 122 (2014) 16–28.

[25] B.-J. He, L. Ding, D. Prasad, Enhancing urban ventilation performance through the development of precinct ventilation zones: a case study based on the Greater Sydney, Australia, Sustain. Cities Soc. 47 (2019) 101472.

[26] R. Giridharan, S.S.Y. Lau, S. Ganesan, et al., Urban design factors influencing heat island intensity in high-rise high-density environments of Hong Kong, Build. Environ. 42 (2007) 3669–3684.

[27] R.H. Sun, Y.H. Lu, X.J. Yang, et al., Understanding the variability of urban heat islands from local background climate and urbanization, J. Clean. Prod. 208 (2019) 743–752.

[28] H. Zhang, S. Zhu, M. Wang, et al., Sky view factor estimation based on 3D urban building data and its application in urban heat island——illustrated by the case of adelaide, Remote Sens. Technol. & Appl. 30 (2015) 899–907.

[29] Y. Hu, Z. Dai, J.M. Guldmann, Modeling the impact of 2D/3D urban indicators on the urban heat island over different seasons: a boosted regression tree approach, J. Environ. Manag. 266 (2020) 110424.

[30] T.M. Logan, B. Zaitchik, S. Guikema, et al., Night and day: the influence and relative importance of urban characteristics on remotely sensed land surface temperature, Remote Sens. Environ. 247 (2020) 111861.

[31] W. Peng, X. Yuan, W. Gao, et al., Assessment of urban cooling effect based on downscaled land surface temperature: a case study for Fukuoka, Japan, Urban Climate 36 (2) (2021) 100790.

[32] M. Belgiu, L. Drăguţ, Random forest in remote sensing: a review of applications and future directions, ISPRS J. Photogrammetry Remote Sens. 114 (2016) 24–31.

[33] K. Deilami, M. Kamruzzaman, Y. Liu, et al., Urban heat island effect: a systematic review of spatio-temporal factors, data, methods, and mitigation measures, Int. J. Appl. Earth Obs. Geoinf. 67 (2018) 30–42.

[34] Y.H. Liu, Y.M. Xu, F.Z. Weng, et al., Impacts of urban spatial layout and scale on local climate: a case study in beijing, Sustain. Cities Soc. 68 (2021) 102767.

[35] E. Mushtaha, S. Shareef, I. Alsyouf, et al., A study of the impact of major Urban Heat Island factors in a hot climate courtyard: the case of the University of Sharjah, UAE. Sustain. Cities Soc. 69 (3) (2021) 102844.

[36] Q. Cao, Q. Luan, Y. Liu, et al., The effects of 2D and 3D building morphology on urban environments: a multi-scale analysis in the Beijing metropolitan region, Build. Environ. 192 (2021) 107635.

[37] J. Chen, W. Zhan, S. Jin, et al., Separate and combined impacts of building and tree on urban thermal environment from two- and three-dimensional perspectives, Build. Environ. 194 (2021) 107650.

[38] S. Alavipanah, J. Schreyer, D. Haase, et al., The effect of multi-dimensional indicators on urban thermal conditions, J. Clean. Prod. 177 (2018) 115–123.

[39] K. Yu, Y. Chen, D. Wang, et al., Study of the seasonal effect of building shadows on urban land surface temperatures based on remote sensing data, Rem. Sens. 11 (5) (2019).

[40] E. Ng, Y. Chao, C. Liang, et al., Improving the wind environment in high-density cities by understanding urban morphology and surface roughness: a study in Hong Kong, Landsc. Urban Plann. 101 (1) (2011) 59–74.

[41] USGS, Landsat 8 (L8) Data Users Handbook, Department of the Interior, U.S. Geological Survey, 2016.

[42] C. Zeng, H. Shen, Li Zhang, Recovering missing pixels for Landsat ETM+ SLC-off imagery using multi-temporal regression analysis and a regularization method, Remote Sens. Environ. 131 (2013) 182–194.

[43] G.S. Golany, Urban design morphology and thermal performance, Atmos. Environ. 30 (1996), 0-465.

[44] J. Konarska, F. Lindberg, A. Larsson, et al., Transmissivity of solar radiation through crowns of single urban trees—application for outdoor thermal comfort modelling, Theor. Appl. Climatol. 117 (2014) 363–376.

[45] C.W. Kent, S. Grimmond, J. Barlow, et al., Evaluation of urban local-scale Aerodynamic parameters: implications for the vertical profile of wind speed and for source areas, Boundary-Layer Meteorol. 164 (2017) 183–213.

[46] I.D. Stewart, T.R. Oke, Local climate zones for urban temperature studies, Bull. Am. Meteorol. Soc. 93 (12) (2012) 1879–1900.

[47] D.A. Artis, W.H. Carnahan, Survey of emissivity variability in thermography of urban areas, Remote Sens. Environ. 12 (1982) 313–329.

[48] J.A. Sobrino, J.C. Jiménez-Muñoz, L. Paolini, Land surface temperature retrieval from LANDSAT TM 5, Remote Sens. Environ. 90 (2004) 434–440.

[49] G. Chander, B.L. Markham, D.L. Helder, Summary of current radiometric calibration coefficients for Landsat MSS, TM, ETM+, and EO-1 ALI sensors, Remote Sens. Environ. 113 (2009) 893–903.

[50] E.M. Abdel-Estoque, O. Mutanga, E. Adam, et al., Detecting Sirex noctilio grey-attacked and lightning-struck pine trees using airborne hyperspectral data, random forest and support vector machines classifiers, ISPRS J. Photogrammetry Remote Sens. 88 (2014) 48–59.

[51] L. Breiman, Statistical modeling: the two cultures (with comments and a rejoinder by the author), Stat. Sci. 16 (2001) 199–231.

[52] M. Belgiu, L. Drăguţ, Random forest in remote sensing: a review of applications and future directions, ISPRS J. Photogrammetry Remote Sens. 114 (2016) 24–31.

[53] J.H. Friedman, Greedy function approximation: a gradient boosting machine, Ann. Stat. 29 (2001) 1189–1232.

[54] T.R. Oke, The urban energy balance, Prog. Phys. Geogr. 12 (4) (1988) 471–508.

[55] I. Charalampopoulos, I. Tsiros, A. Chronopoulou-Sereli, et al., Analysis of thermal bioclimate in various urban configurations in Athens, Greece, Urban Ecosyst. 16 (2) (2013) 217–233.

[56] L.V. Hove, C. Jacobs, B.G. Heusinkveld, et al., Temporal and spatial variability of urban heat island and thermal comfort within the Rotterdam agglomeration, Build. Environ. 83 (2015) 91–103.

[57] C. Berger, J. Rosentreter, M. Voltersen, et al., Spatio-temporal analysis of the relationship between 2D/3D urban site characteristics and land surface temperature, Remote Sens. Environ. 193 (2017) 225–243.